

光纤激光 GH3128 搭接接头高温力学性能研究

袁振飞¹, 蒋劲², 程智伟¹, 杜欣¹, 祁百鑫¹, 武强^{1*}, 杨顺华^{2**}, 肖荣诗¹¹北京工业大学材料与制造学部高功率及超快激光先进制造实验室, 北京 100124;²中国空气动力研究与发展中心高超声速冲压发动机技术重点实验室, 四川 绵阳 621000

摘要 基于侧吹保护条件下的光纤激光非穿透深熔焊接工艺, 模拟了构件的服役环境, 对 GH3128 搭接接头进行了不同循环次数的 900 °C 真空热处理, 并对接头组织和显微硬度、室温与高温拉伸及蠕变拉伸性能进行了分析测试, 通过分析组织与断口, 对 GH3128 搭接接头的高温力学性能进行了评估。研究表明, 与无热处理接头相比, 热处理后的接头的室温与高温拉伸性能分别提升了 35% 和 20%, 蠕变性能大幅提高。接头组织分析结果表明: 热处理后的接头枝状组织消除, 晶粒呈粗大等轴晶状态; 各断口均呈现出“抛物线”状韧窝, 开口方向与拉伸力方向一致, 呈韧性断裂特征, 且无显微裂纹产生; 热处理次数对接头显微硬度、室温及高温拉伸性能的影响不大; 随着热处理次数的增加, 接头蠕变性能呈减小趋势。

关键词 光纤光学; 激光焊接; GH3128; 搭接接头; 高温拉伸; 蠕变性能

中图分类号 TG442

文献标志码 A

DOI: 10.3788/CJL202249.2106003

1 引言

GH3128 镍基高温合金具有较强的抗腐蚀、抗氧化能力和较高的抗疲劳强度等优点, 被广泛应用于发动机燃烧室、进气道、尾喷管等高温部件中^[1-2]。光纤激光焊接具有柔性高、速度快、焊缝深宽比大、焊后变形小及可在大气环境中实施等诸多优势, 在工业领域中被广泛应用^[3-5]。航天领域内的主动热防护结构通常由高温合金制造, 搭接接头是激光焊接工艺制造的主动热防护结构的主要接头形式^[6]。主动热防护构件工作时的热负荷条件苛刻, 且面临重复服役新需求, 这就需要对搭接接头在多次热服役时的高温力学性能及组织演变规律有清晰的认识, 使得焊缝可靠性评估的新要求得到满足^[7-8]。

在高温合金焊缝高温力学性能及组织演变方面, Ram 等^[9]对脉冲 Nd:YAG 激光焊接的 2 mm 厚的 Inconel718 高温合金对接试样进行了高温组织及力学性能测试, 发现长时间时效处理后的焊缝组织发生明显变化, 且焊缝高温拉伸性能也发生变化。Ren 等^[10]发现, 当 Inconel617 高温合金的高温时间大于 500 h 时, 晶界处不连续分布的 M_6C 和 $M_{23}C_6$ 碳化物的粗化将降低焊缝的室温强度, 不连续 $M_{23}C_6$ 碳化物的大量析出和晶界 $M_{23}C_6$ 碳化物间距的增加能提高焊缝的冲击韧性, 而 M_6C 碳化物会降低冲击韧性。Li 等^[11]发现, 镍基高温合金 720Li-IN718 异质接头焊接

区的高温抗疲劳裂纹的扩展能力不如母材, 疲劳裂纹的扩展速率随着试验温度的升高而升高。王媛媛等^[12]研究了温度对 625 镍基高温合金焊接接头低周疲劳行为的影响, 发现 760 °C 下的疲劳变形呈循环硬化趋势, 疲劳裂纹以穿晶和沿晶混合方式扩展。刘杨等^[13]研究了镍基高温合金 DD407/IN718 对接接头组织及高温拉伸变形行为, 发现接头在 650 °C 高温拉伸下的屈服和抗拉强度低于母材。张冬旭等^[14]发现, GH3230 高温合金钨极氩弧填丝焊对接接头在高温拉伸和高温蠕变试验后的断口形貌与母材基本一致, 分别为韧窝型和沿晶断裂。徐殿峰^[15]测试了 GH3128 镍基合金材料在不同温度和不同拉力下的蠕变曲线, 结果显示, 温度越高, 蠕变性能越差。由此可见, 国内外学者着重研究高温合金对接接头及母材的高温力学性能、组织演变及长时间蠕变行为。GH3128 作为固溶强化型镍基高温合金, 由单相奥氏体组成, 经长期高温时效可能会析出 M_6C 和 $M_{23}C_6$ 相。关于 GH3128 搭接接头在高温短时重复热处理条件下的焊缝组织演变及高温力学性能变化规律的研究鲜有报道。

在主动热防护构件工作过程中, 在流道内高温高压燃料作用下, 搭接接头的受力方式及服役状态与对接接头明显不同。搭接接头主要在结合面处以撕裂方式横向断裂, 而对接接头主要在熔合线或缺陷处纵向断裂, 搭接接头的力学性能与其受力方式和结构形式密切相关。搭接接头的激光非穿透焊接工艺特点导致

收稿日期: 2022-01-11; 修回日期: 2022-02-22; 录用日期: 2022-03-07

基金项目: 国家自然科学基金面上项目(51775009)、高超声速冲压发动机技术重点实验室开放课题(STSMY-KFKT-2020003)

通信作者: *jlwuqiang@bjut.edu.cn; **yangshunhua@cardc.cn

焊缝中弥散状分布的气孔缺陷很难被完全消除^[16-17]。因此,针对主动热防护构件的接头形式、高温短时服役特点及重复服役的新需求,开展不同真空热处理次数下的 GH3128 搭接接头组织及力学性能的研究,可为高温服役条件下的主动热防护构件光纤激光搭接焊缝的性能评估提供参考。

本文基于侧吹保护条件下的光纤激光非穿透深熔焊接工艺,通过对搭接接头进行不同循环次数的 900 °C 真空热处理,分析了接头组织及显微硬度,并对接头的室温和高温拉伸性能及蠕变拉伸性能进行了测试,分析了断口形貌,完成了 GH3128 搭接接头高温力学性能的研究。

2 试验方法与设备

试验材料为固溶态 GH3128 板材,上板尺寸为 200 mm × 150 mm × 1 mm,下板尺寸为 200 mm × 150 mm × 2 mm,材料表面采用拉丝布去掉表面氧化

膜,焊前用丙酮清洗表面。

焊接试验装置示意图如图 1 所示。光源采用波长为 1060~1070 nm 的 YLS-6000 光纤激光器,其光束聚焦参数 $K_f = 8 \text{ mm} \cdot \text{mrad}$,传输光纤的芯径为 200 μm ,输出耦合准直镜的焦距为 200 mm,聚焦透镜的焦距为 300 mm。采用旁轴喷嘴保护,焊接方式为拖焊(保护气在前,激光头在后),采用高纯 Ar 气(体积分数为 99.999%)作为保护气体,流量为 8 L/min;喷嘴内径为 8 mm,光气间距为 $D = 2 \text{ mm}$,喷嘴输出长度为 $L = 6 \text{ mm}$,保护气输出角度 $\theta = 50^\circ$ 。焊接工艺参数如下:激光输出功率 $P = 1500 \text{ W}$,焊接速度 $V = 2 \text{ m/min}$,离焦量 $\Delta F = 0$ 。

焊后在同一试样上制备图 2 所示的力学性能测试试样(室温拉伸试样、高温拉伸试样与蠕变试样),其中 t 为厚度。对于高温拉伸试样与蠕变试样,在上板和下板拉伸试样的端头处补焊加强块(材料为 GH3128),这样可保证拉伸试验过程中拉伸孔位置处的强度。将

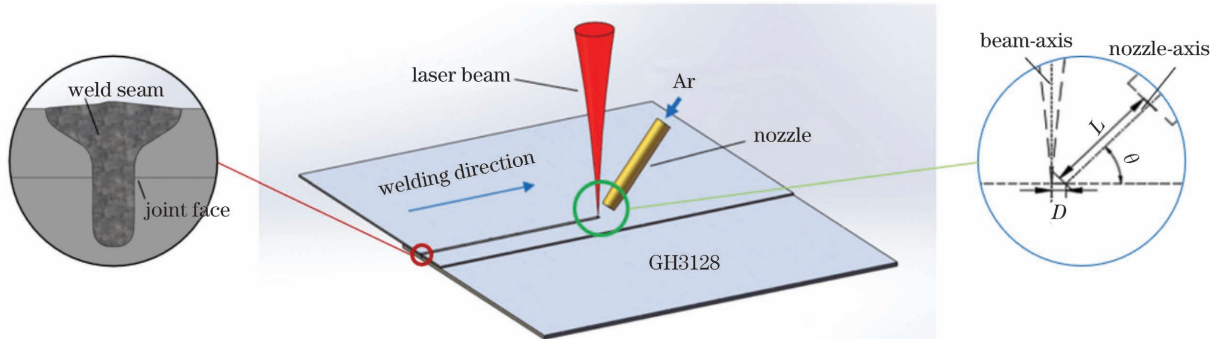


图 1 试验装置示意图

Fig. 1 Schematic of test device

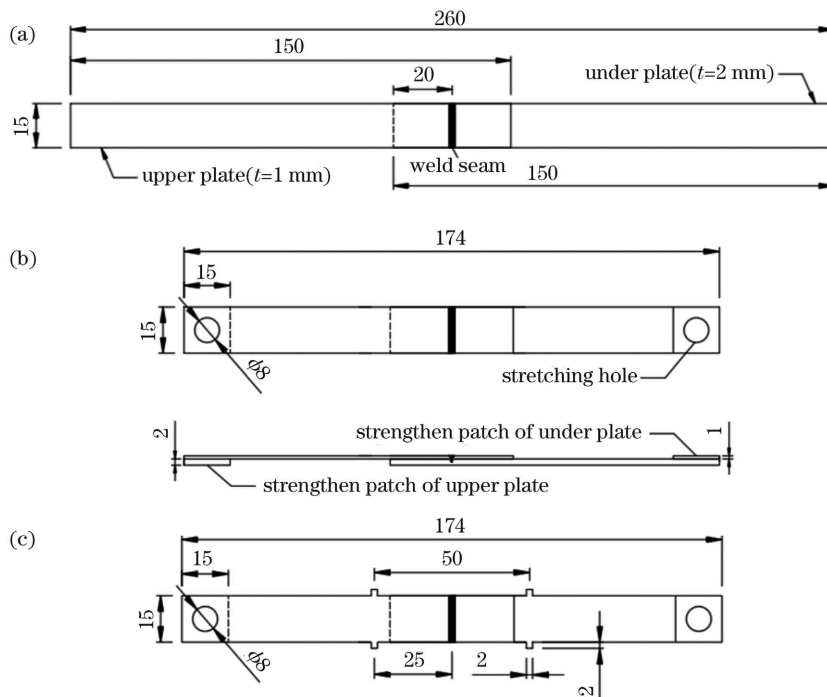


图 2 拉伸试样的设计图。(a)室温拉伸试样;(b)高温(900 °C)拉伸试样;(c)蠕变拉伸试样

Fig. 2 Drawings of tensile specimens. (a) Room-temperature tensile specimen; (b) high-temperature (900 °C) tensile specimen; (c) creep tensile specimen

各试样分为 4 批,一批不作热处理,另外三批分别进行 1 次、3 次及 5 次热处理,热处理设备为 VBFV-300 真空炉。热处理参数如图 3 所示,在 3600 s 内均匀升温

至 900 °C,在 900 °C 保温 1000 s,然后随炉冷却至室温,并根据热处理次数要求进行相应次数的循环热处理。

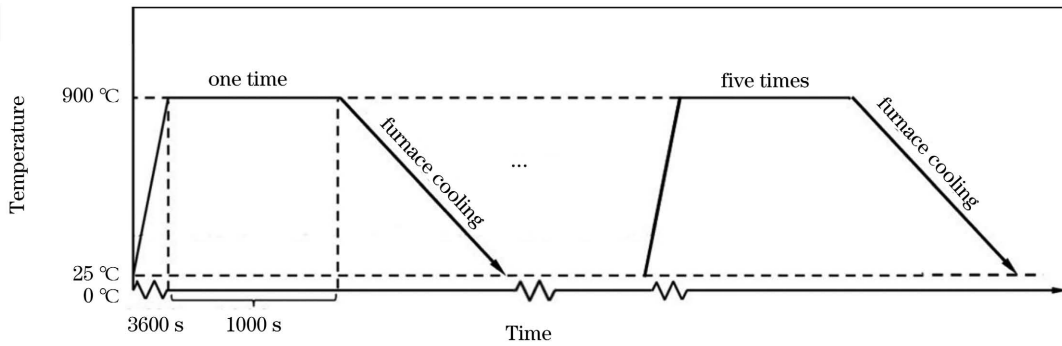


图 3 拉伸试样的真空热处理温升曲线图

Fig. 3 Temperature rise curve of tensile specimens during vacuum heat treatment

针对不同批次的试样进行金相试样制备,采用王水(6 mL HCl+2 mL HNO₃)腐蚀焊缝,用乙醇清洗焊缝。采用光学显微镜观测焊缝形貌;采用扫描电子显微镜(SEM)观测断口及组织;采用显微硬度仪检测焊缝硬度,载荷为 100 g,加载时间为 15 s。采用高温拉伸试验机对各批次试样进行室温拉伸性能测试;采用拉伸试验机对焊缝进行 900 °C 高温拉伸性能测试;采用 RD-100 设备对焊缝进行 900 °C 蠕变性能测试,测试时拉力为 800 N,时间为 6 h。

3 结果与分析

3.1 焊缝形貌及组织

搭接接头焊缝形貌及不同热处理条件下的焊缝组织如图 4 所示。接头为深熔焊接中典型的“钉头”形焊缝形貌,焊缝熔深为 2.06 mm,结合面宽度约为 550 μm,焊缝中有圆形零星气孔,位于结合面下部的焊缝根部附近,直径为 50~150 μm 不等。分别观察不同热处理条件下焊缝上部、结合面处及焊缝下部的

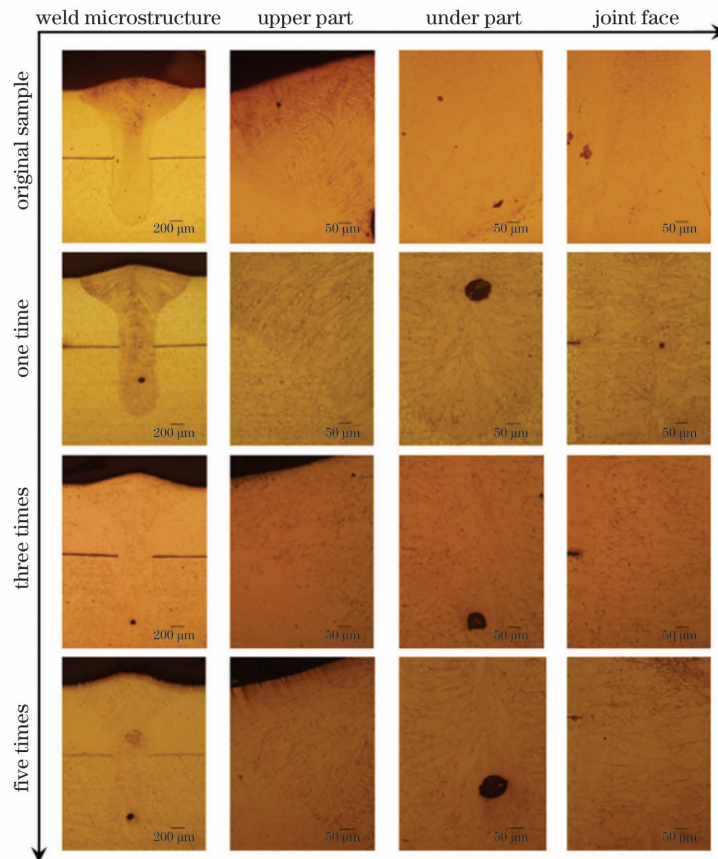


图 4 不同热处理次数下 GH3128 搭接焊缝的典型组织

Fig. 4 Typical microstructures of GH3128 lap welds under different numbers of heat treatment cycles

组织。在没有经过热处理的接头中,接头组织主要为柱状晶,柱状晶沿焊缝中心线呈对称分布,生长方向与熔合线垂直。与结合面处及下部焊缝处的柱状晶相比,焊缝上部“钉头”附近的柱状晶较长。在经过真空热处理后,各热处理次数下的焊缝接头的晶粒均呈“粗化”现象,在气孔周围无显微裂纹产生。

3.2 力学性能

3.2.1 显微硬度

焊缝显微硬度的测试位置如图 5 所示,分别在焊缝中心位置及结合面上、下方各 0.5 mm 距离处,测试间隔均为 0.1 mm。显微硬度分布如图 6 所示。其中,接头的显微硬度高于母材,母材(BM)硬度约为 235 HV,焊缝(WZ)硬度约为 255 HV。由图 6 可知,热处理次数对焊缝各部位及母材的硬度没有明显影响。无论是纵向[图 6(a)]还是横向[图 6(b)、(c)]的显微硬度分布,熔合线附近的硬度会出现高点,焊缝中部的显微硬度有波动。这是由于激光焊接速度快,

GH3128 热传导系数高,因此熔合线附近的过冷度大,晶粒细小,从而硬度偏高。另外,激光焊接时的凝固速率快,焊缝熔合区的强化相析出不充分,导致焊缝熔化区域内的显微硬度出现波动。

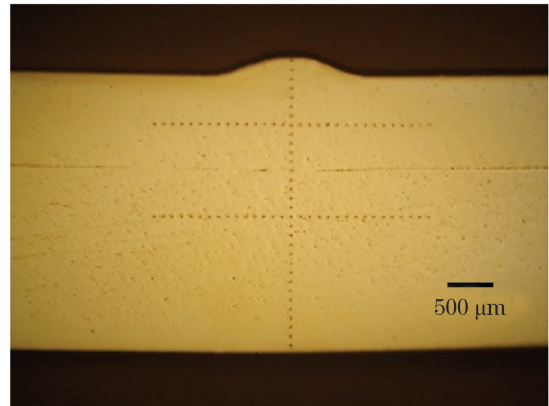


图 5 显微硬度的测试位置

Fig. 5 Microhardness test locations

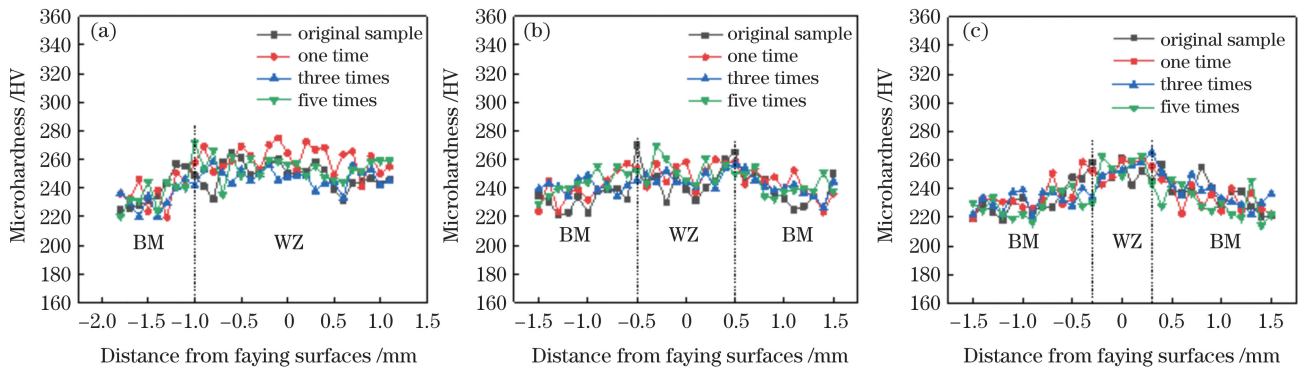


图 6 不同热处理次数下搭接接头的显微硬度分布。(a)焊缝中心位置处;(b)上板处;(c)下板处

Fig. 6 Microhardness distributions of lap joints under different numbers of heat treatment cycles. (a)At center of weld; (b)at upper plate; (c)at under plate

3.2.2 拉伸性能

不同热处理次数下 GH3128 搭接接头的室温及 900 °C 高温拉伸性能如图 7 所示(每个参数下有 3 个测试样),所有接头均在焊缝结合面处断裂(图 8)。可以看出:与室温拉伸强度相比, GH3128 搭接接头 900 °C 高温抗拉强度下降了 50%左右(其中 0、1、3、5 次热处理后的高温拉伸强度分别约为室温的 54.13%、46.25%、50.02%、47.82%);经过不同次数热处理后,接头的室温拉伸强度由没有经过热处理的 4772 N 分别提高到 6462 N(1 次热处理)、6281 N(3 次热处理)和 6564 N(5 次热处理),热处理使接头室温拉伸强度提高了 31.6%~37.6%。接头的高温拉伸测试结果显示,经过不同次数热处理后,接头 900 °C 高温拉伸强度由无热处理的 2583 N 分别提高到 2989 N(1 次热处理)、3142 N(3 次热处理)和 3139 N(5 次热处理),热处理使接头高温拉伸强度提高了 15.7%~21.6%。采用图 3 所示的真空热处理工艺可提高接头的拉伸强度,但热处理次数对接头的室温和高温拉伸强度的影响不大。所有拉伸试样均由同一焊接试样加

工而成,气孔数量和形态的差异性不大,它们对各试样接头性能的影响基本无差异,所以接头性能出现差异的原因与焊缝组织密切相关。

在 900 °C 高温环境下, GH3128 的屈服强度急剧降低,仅为室温条件下 GH3128 屈服强度的 50%,拉

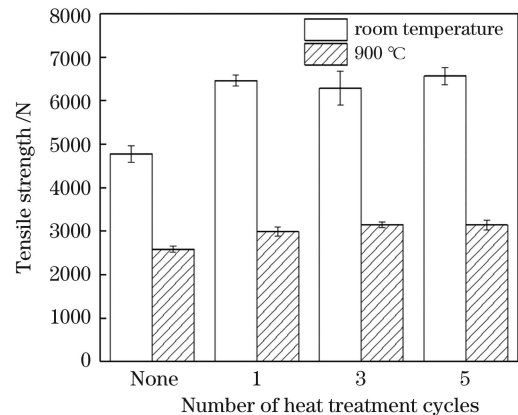


图 7 不同热处理条件下 GH3128 搭接接头的拉伸性能

Fig. 7 Tensile properties of GH3128 lap joints under different heat treatment conditions

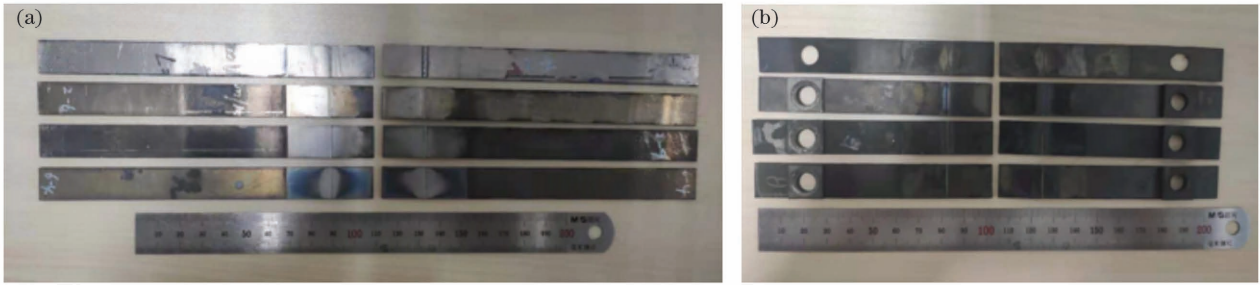


图 8 不同拉伸断裂试样。(a)室温拉伸试样;(b) 900 °C 拉伸试样

Fig. 8 Different tensile fracture specimens. (a) Room-temperature tensile specimens; (b) 900 °C tensile specimens

伸强度也随之降低。热处理除了影响焊缝组织外,还有利于焊缝内部应力的释放,提高了焊缝的拉伸强度。图 7 相关数据显示,热处理对搭接接头高温拉伸强度的增强作用明显弱于其对室温拉伸强度的增强作用。这是由于随着测试温度的升高,在韧性断裂机制下, GH3128 的屈服强度逐渐降低,因此拉伸测试时裂纹更容易萌生并扩展。另外,在 900 °C 高温拉伸测试期间,接头的残余应力逐渐得到释放,这也有助于提高非热处理试样的高温拉伸强度,热处理试样和非热处理试样高温拉伸测试时的强度差值减小。因此,在进行高温拉伸测试时,热处理对试样拉伸强度的增强作用不如室温测试条件下显著。

通过对断口形貌进行观测,比较分析没有经过

热处理和经过 5 次热处理后的室温和高温接头断口形貌(图 9)。发现焊缝断面上分布少量气孔[图 9(a)~(d)],且经过 5 次热处理后,在室温和高温拉伸焊缝断面上,气孔数量没有增加,也没有出现裂纹。各气孔内壁均有涡流痕迹,形状呈球形[图 9(a₂)~(d₂)],这是工艺特征型气孔的主要特征^[18],气孔直径约为 150 μm。其中,各断口上呈现出“抛物线”状韧窝,开口方向与拉伸力方向一致[图 9(a₁)~(d₁)]。由室温拉伸试样的断口形貌可以看出,没有经过热处理的接头断口的韧窝宽度约为 1.2 μm,而经过 5 次热处理后的接头断口的韧窝宽度约为 0.85 μm。高温拉伸试样的接头断口的韧窝宽度约为 2.2 μm。

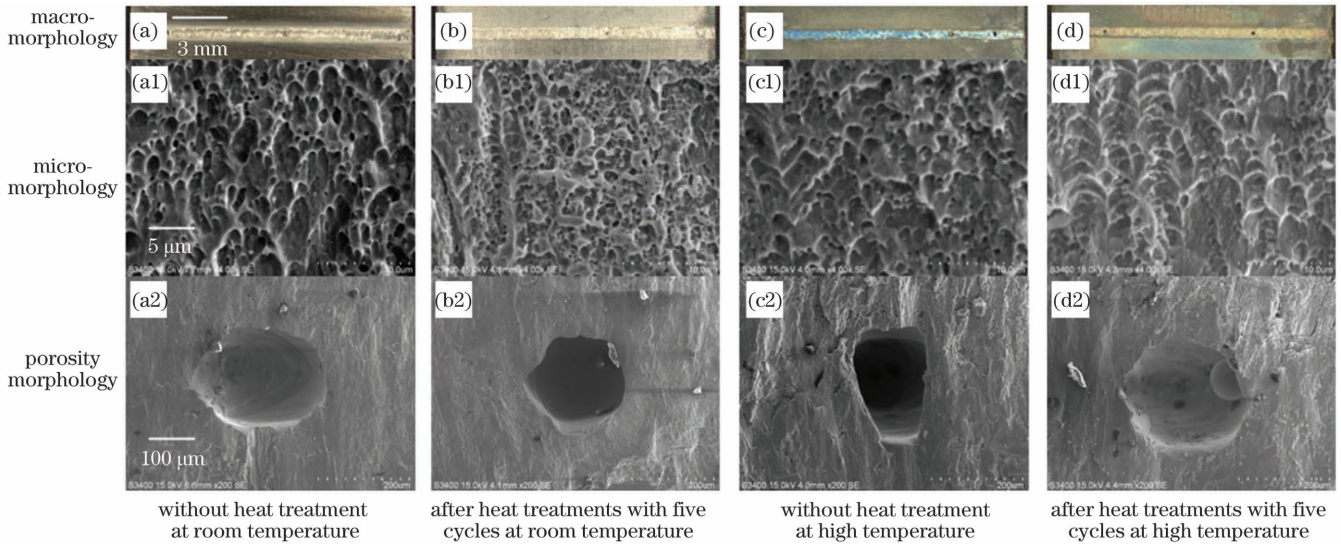


图 9 拉伸断口形貌

Fig. 9 Tensile fracture morphologies

3.2.3 接头的高温蠕变性能分析

对不同热处理条件下的焊缝接头进行蠕变拉伸测试,测试曲线如图 10 所示,其中测试温度为 900 °C,测试拉力为 800 N。可以看出,对 GH3128 激光焊接接头进行短时蠕变测试时,各热处理次数条件下的接头均未出现蠕变第三时期(应变随时间的增加加速增长的时期),仅有蠕变第一时期(应变随时间的增加减速增长的时期)与第二时期(应变随时间的增加稳定增长的时期),经过热处理的接头的蠕变第一与第二时期的性能有所提升^[15]。

其中,无热处理接头的蠕变曲线斜率最大,其最大蠕

变应变为 1.12。而对于热处理后的接头,虽然随着热处理次数的增加,其曲线斜率有轻微增大趋势,但均远小于无热处理试样的蠕变曲线斜率,并且各热处理次数下接头的蠕变曲线斜率的变化不大,经过 5 次热处理后,其最大蠕变应变由 1 次热处理试样的 0.05% 上升为 0.12%。

由于焊缝结合面处焊缝的组织对搭接接头的力学性能具有重要的影响,因此对没有经过热处理的接头和分别经过 1 次和 5 次热处理的接头在结合面处的组织进行 SEM 观测,检测位置分别在搭接接头结合面的中心和结合面中线两侧(图 11)。

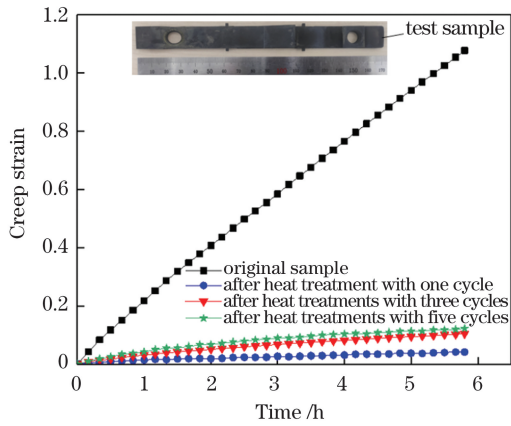


图 10 GH3128 搭接接头在 900 °C 下的蠕变曲线
Fig. 10 Creep curves of GH3128 lap joint at 900 °C

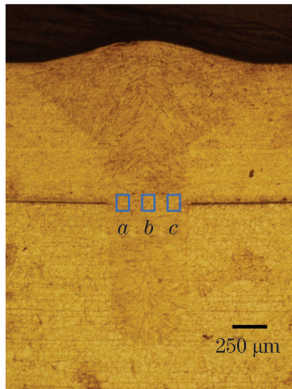


图 11 SEM 检测位置
Fig. 11 Detecting positions on joint surface by SEM

不同热处理次数下各检测位置的组织演变如图 12 所示。没有经过热处理的接头在结合面中心位置处的组织主要是小尺寸的柱状枝晶，结合面中线两侧的柱状枝晶组织的尺寸略大，并且晶粒细长，生长方向与结合面基本平行。图 11 的焊缝形貌为典型的激光深熔焊接“钉头”形貌，结合面位于焊缝“钉头”的下部。此时，熔合线基本与搭接结合面垂直，在熔池快速冷却条件下，晶粒生长方向与熔合线垂直。而在焊缝中部较小的冷却梯度及两侧柱状枝晶相向生长的条件下，焊缝中部出现较小尺寸的等轴晶。

经过 1 次热处理后，接头结合面三个检测位置处均出现明显的粗大等轴晶的晶界，而且枝晶组织有消融迹象[图 12(a₂)~(c₂)]。在经过 5 次热处理后，结合面各位置处的柱状枝晶组织完全消融在等轴晶粒内，粗大等轴晶的晶界明显[图 12(a₃)~(c₃)]。不同热处理次数下结合面处均无显微裂纹产生。晶粒尺寸的增大可有效阻碍位错滑动与晶界运动，提升接头的抗变形能力，进而提升搭接接头的高温拉伸和高温蠕变性能。另外，经过热处理后，接头的残余应力获得释放，这有助于提高焊缝的抗拉强度。因此，经过热处理后，GH3128 搭接接头的室温拉伸、高温拉伸及蠕变拉伸性能得到提升^[19-20]。

4 结 论

不同热处理次数下的 GH3128 搭接接头，与无热处理的接头相比，其室温与高温拉伸性能分别提升了

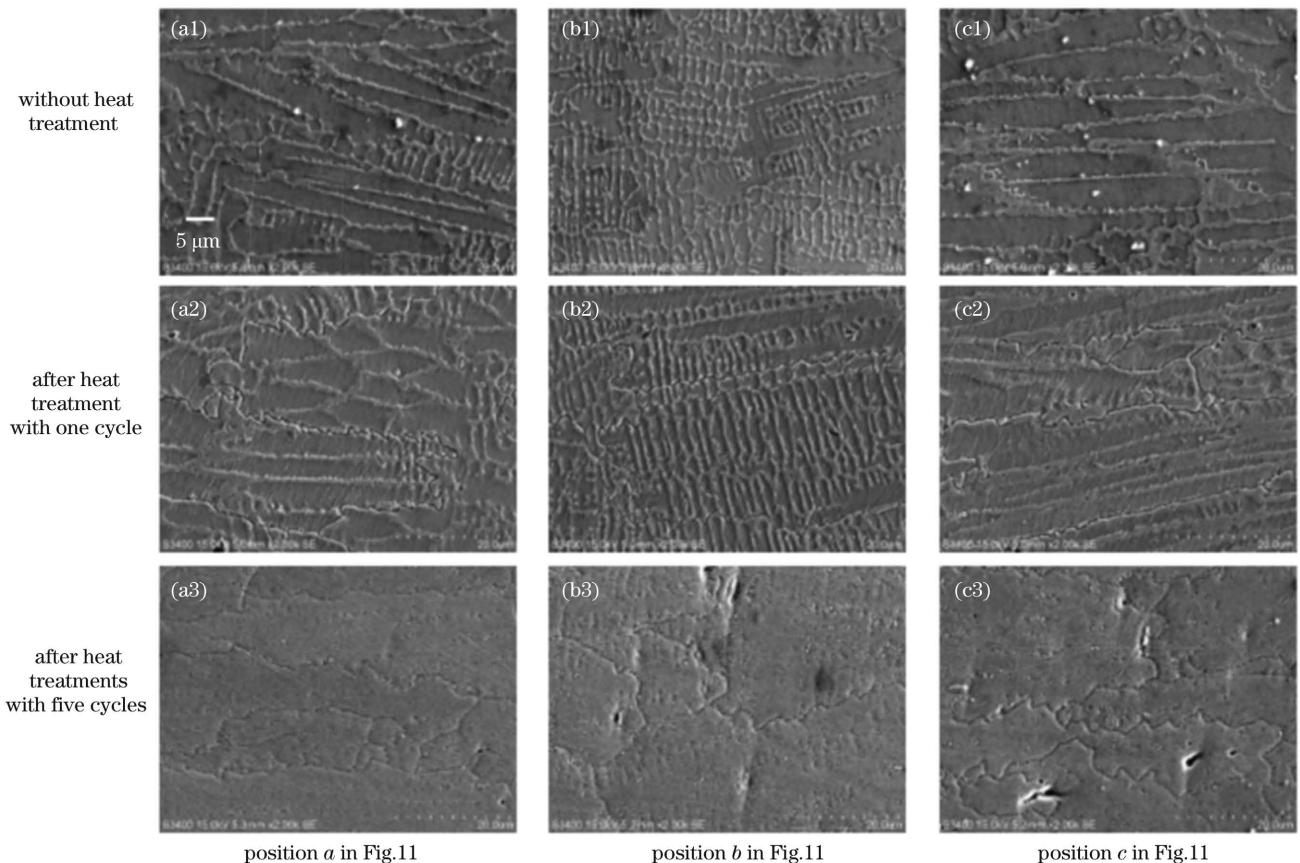


图 12 结合面处焊缝组织的 SEM 图

Fig. 12 SEM images of weld microstructure at joint surface

31.6%~37.6%和15.7%~21.6%。同时,接头的蠕变性能大幅提高。其中,经过5次热处理后,接头的最大蠕变应变由无热处理试样的1.08%下降为0.12%。

接头组织分析结果表明,热处理后的接头晶粒变大,晶粒内的枝晶组织逐渐消融,经过5次热处理后,接头晶粒为粗大的等轴晶粒,枝晶组织完全消融。随着热处理次数的增加,接头的蠕变性能呈下降趋势。其中,经过5次热处理后,接头的最大蠕变应变由1次热处理试样的0.05%上升为0.12%。

不同热处理次数下的搭接接头结合面无显微裂纹产生。接头的室温及高温拉伸断口均出现“抛物线”状的韧窝,开口方向与拉伸力方向一致,呈韧性断裂特征。

参 考 文 献

- [1] Zhang L X, Chang Q, Sun Z, et al. Diffusion bonding of hydrogenated TC4 alloy and GH3128 superalloy using composite interlayers[J]. Journal of Materials Processing Technology, 2019, 274: 116266.
- [2] Zhao X, Yuan K, Zhou Y, et al. Research on the high-temperature hot compressive deformation behavior of Ni-based superalloy GH3128[J]. Journal of Pressure Vessel Technology, 2017, 139(2): 021401.
- [3] 顾冬冬, 张红梅, 陈洪宇, 等. 航空航天高性能金属材料构件激光增材制造[J]. 中国激光, 2020, 47(5): 0500002. Gu D D, Zhang H M, Chen H Y, et al. Laser additive manufacturing of high-performance metallic aerospace components[J]. Chinese Journal of Lasers, 2020, 47(5): 0500002.
- [4] 孙文昊, 范永强, 张国涛, 等. SiC_p/Al 复合材料的激光焊接接头组织与性能对比[J]. 中国激光, 2021, 48(10): 1002105. Sun W H, Fan Y Q, Zhang G T, et al. Comparison of structure and performance of laser welded joints of SiC_p/Al composite materials[J]. Chinese Journal of Lasers, 2021, 48(10): 1002105.
- [5] Gao M, Chen C, Hu M, et al. Characteristics of plasma plume in fiber laser welding of aluminum alloy[J]. Applied Surface Science, 2015, 326: 181-186.
- [6] 曹政, 姜仁杰, 杜伟哲, 等. 薄壁结构激光焊接随焊高频冲击变形控制[J]. 中国激光, 2020, 47(9): 0902003. Cao Z, Jiang R J, Du W Z, et al. Distortion control by in-site high frequency peening in laser welding of thin-walled structures[J]. Chinese Journal of Lasers, 2020, 47(9): 0902003.
- [7] 蒋劲. 超燃冲压发动机燃烧室再生冷却研究[D]. 西安: 西北工业大学, 2006: 1-4. Jiang J. Research on regenerative cooling of scramjet combustor[D]. Xi'an: Northwestern Polytechnical University, 2006: 1-4.
- [8] 赵书军, 马云峰. 微小通道主动冷却结构焊接工艺[C]//中国航天第三专业信息网第三十七届技术交流会暨第一届空天动力联合会会议. 北京: 中国航天第三专业信息网, 2016: 377-380. Zhao S J, Ma Y F. Welding process of micro channel active cooling structure[C]//The 37th Technical Exchange Conference and the first Joint Conference of Space and Space Power. Beijing: Aerospace Propulsion Technology Information Society, 2016: 377-380.
- [9] Ram G D J, Reddy A V, Rao K P, et al. High temperature mechanical properties of Inconel 718 pulsed Nd-YAG laser welds[J]. Materials at High Temperatures, 2006, 23(1): 29-37.
- [10] Ren W J, Lu F G, Nie P L, et al. Effects of the long-time thermal exposure on the microstructure and mechanical properties of laser weldings of Inconel 617[J]. Journal of Materials Processing Technology, 2017, 247: 296-305.
- [11] Li H Y, Huang Z W, Bray S, et al. High temperature fatigue of friction welded joints in dissimilar nickel based superalloys[J]. Materials Science and Technology, 2007, 23(12): 1408-1418.
- [12] 王媛媛, 陈立佳, 王宝森. 温度对625镍基高温合金焊接接头低周疲劳行为的影响[J]. 金属学报, 2014, 50(12): 1485-1490. Wang Y Y, Chen L J, Wang B S. Influence of temperature on low-cycle fatigue behavior of Inconel 625 Nickel-based superalloy welding joint[J]. Acta Metallurgica Sinica, 2014, 50(12): 1485-1490.
- [13] 刘杨, 王磊, 宋秀, 等. DD407/IN718 高温合金异质焊接接头的组织及高温变形行为[J]. 金属学报, 2019, 55(9): 1221-1230. Liu Y, Wang L, Song X, et al. Microstructure and high-temperature deformation behavior of dissimilar superalloy welded joint of DD407/IN718[J]. Acta Metallurgica Sinica, 2019, 55(9): 1221-1230.
- [14] 张冬旭, 刘大顺, 朱西平, 等. GH3230 高温合金氩弧焊接接头的组织与高温性能[J]. 机械工程材料, 2013, 37(12): 35-37, 41. Zhang D X, Liu D S, Zhu X P, et al. High-temperature properties and microstructure of argon-arc welded joint of GH3230 superalloy[J]. Materials for Mechanical Engineering, 2013, 37(12): 35-37, 41.
- [15] 徐殿峰. GH3128 高温合金中间换热器冷却管蠕变特性研究[D]. 秦皇岛: 燕山大学, 2019: 7-21. Xu D F. Study on creep properties of GH3128 superalloy cooling tube in intermediate heat exchanger[D]. Qinhuangdao: Yanshan University, 2019: 7-21.
- [16] Jiang M, Chen X, Chen Y B, et al. Mitigation of porosity defects in fiber laser welding under low vacuum[J]. Journal of Materials Processing Technology, 2020, 276: 116385.
- [17] Chen X, Pang S Y, Shao X Y, et al. Sub-microsecond vapor plume dynamics under different keyhole penetration regimes in deep penetration laser welding[J]. Journal of Physics D: Applied Physics, 2017, 50(20): 205601.
- [18] Wu Q, Xiao R S, Zou J L, et al. Weld formation mechanism during fiber laser welding of aluminum alloys with focus rotation and vertical oscillation[J]. Journal of Manufacturing Processes, 2018, 36: 149-154.
- [19] Woo K D, Kim S W, Yang C H, et al. Effects of grain size on high temperature deformation behavior of Al-4Mg-0.4Sc alloy[J]. Materials Letters, 2003, 57(13/14): 1903-1909.
- [20] Peng H L, Li X F, Chen X, et al. Effect of grain size on high-temperature stress relaxation behavior of fine-grained TC4 titanium alloy[J]. Transactions of Nonferrous Metals Society of China, 2020, 30(3): 668-677.

High-Temperature Mechanical Properties of Fiber Laser Welding GH3128 Overlap Joints

Yuan Zhenfei¹, Jiang Jin², Cheng Zhiwei¹, Du Xin¹, Qi Baixin¹, Wu Qiang^{1*},
Yang Shunhua^{2**}, Xiao Rongshi¹

¹High-Power and Ultrafast Laser Manufacturing Laboratory, Faculty of Materials and Manufacturing,
Beijing University of Technology, Beijing 100124, China;

²Science and Technology on Scramjet Laboratory, China Aerodynamics Research and Development Center,
Mianyang 621000, Sichuan, China

Abstract

Objective GH3128 has the benefits of strong heat, pressure, and corrosion resistance, and is extensively employed in high-temperature components of active thermal protection structures in the aerospace field. Laser welding is the primary manufacturing process of active thermal protection components, and the lap joint is the primary joint form. The thermal load condition of the active thermal protection components is harsh, which puts forward higher demands on the high-temperature mechanical properties of lap joints. In this study, in view of the joint forms and high-temperature short-time work characteristics of active thermal protection components, the microstructure and mechanical properties of GH3128 lap joints under different vacuum heat treatment conditions are investigated on the basis of fiber laser non-penetrating deep fusion welding process under the condition of side blowing protection.

Methods The test materials are GH3128 plates with the solution state, the upper plates' size is 200 mm × 150 mm × 1 mm, and the lower plates' size is 200 mm × 150 mm × 2 mm. The light source is a fiber laser with a wavelength of 1060–1070 nm. The beam focusing parameter is $K_f = 8 \text{ mm} \cdot \text{mrad}$, the transmission fiber core diameter is 200 μm , the output coupling collimator's focal length is 200 mm, and the focusing lens' focal length is 300 mm. High purity Ar gas is employed as the protection gas, and the flow rate is 8 L/min. The nozzle's inner diameter is 8 mm, the phosgene spacing is 2 mm, the nozzle's output length is 6 mm, and the protective gas output angle is 50°. The welding process parameters are as follows: the laser output power is 1500 W, the welding speed is 2 m/min, and the defocusing is 0. After welding, the mechanical properties of GH3128 lap joints are tested, and the GH3128 lap joints are subjected to 900 °C vacuum heat treatment with different cycles.

The weld is corroded with aqua regia (6 mL HCl + 2 mL HNO₃), cleaned with alcohol, and used as a metallographic sample. An optical microscope is employed to observe the weld morphology. The fracture and microstructure are observed using a scanning electron microscope. The weld hardness is tested using a microhardness tester with a load of 100 g and loading time of 15 s. The tensile testing machine is employed to test the tensile properties of each batch of samples at room temperature. The tensile testing machine is employed to test the weld's tensile properties at 900 °C. At 900 °C, the equipment is employed to test the weld's creep property. The tensile force is 800 N and the time is 6 h.

Results and Discussions The joints are typical “nail head” weld shapes in deep fusion welding, and there are circular sporadic pores near the weld's root at the joint surface's lower part. The joint microstructures are primarily columnar crystals, symmetrically dispersed along the weld center line, and the growth direction is perpendicular to the fusion line (Fig. 4). The columnar crystals near the “nail head” at the upper part of the weld are longer compared with the columnar crystals at the joint surface and the lower weld. After vacuum heat treatments with different cycles, the weld joint's grain size becomes larger and there are no microcracks around the porosity.

The microhardness of lap joints under different heat treatment cycles is higher than that of the base metal, and the microhardnesses of the weld joints and base metal have no visible change (Fig. 6). The tensile properties demonstrate that the GH3128 lap joints' tensile strength at high temperatures decreases by about 50% compared to that at the room temperature. After different heat treatments, the joint's tensile strength at the room temperature increases by about 35%. The joint's tensile strength increases by about 20% at 900 °C (Fig. 7). Vacuum heat treatment can enhance the joints' tensile strength, but the number of heat treatment cycles has little impact on the joints' tensile strength at room temperature and high temperature. The creep property test findings demonstrate that the creep curve's slope of joints without heat treatment is the largest. The slope of the joints' curves after heat treatment increases slightly with the increase in numbers of heat treatment cycles, but it is far less than the slope of the specimen's creep curves without heat treatment (Fig. 10).

The microstructure of lap joint faces after heat treatments with different cycles is observed and examined. The

findings demonstrate that the microstructure at the joints' central position without heat treatment is primarily made of small columnar dendrites, while the columnar dendrite structure at both sides of the central line of the joints is slightly larger in size. After the first heat treatment, the grain boundaries of coarse equiaxed grains appears at each position of the joint interface, and the dendrite structure demonstrates the sign of melting. After heat treatments with five cycles, the columnar dendrite structure at each position of the interface melts within the equiaxed grain. After each heat treatment, there is no microcracks on the bonding surface (Fig. 12). After heat treatment, the joints' coarse equiaxed grain may be the reason for enhancing of tensile and creep properties of joints at high temperatures.

Conclusions Compared with the joints without heat treatment, the tensile properties of GH3128 lap joints at room temperature and high temperature increase by 35% and 20%. Simultaneously, the joints' creep property is significantly enhanced, and the joints' maximum creep strain decreases from 1.08% (without heat treatment) to 0.12% (after heat treatments with five cycles). The analysis of the joints' microstructure demonstrates that the joints' grain size becomes larger and the dendrite structure in the grain is gradually melted after heat treatments with five cycles. After heat treatments with five cycles, the joints' microstructure is coarse equiaxed grain, and the dendrite structure is entirely melted. The joints' fracture morphology demonstrates that there are "parabolic" dimples on each fracture, and the opening direction is consistent with the direction of the tensile force, demonstrating ductile fracture characteristics without microcracks. The number of heat treatment cycles has little impact on the microhardness, and tensile properties at room temperature and high temperature. With the increase in the number of heat treatment cycles, the joints' creep properties decrease, and the joints' maximum creep strain increases from 0.05% (after heat treatment with one cycle) to 0.12% (after heat treatments with five cycles).

Key words fiber optics; laser welding; GH3128; overlap joint; high temperature tension; creep property